Journal of the Virtual Explorer, 2004
Volume 15
Paper 4
http://virtualexplorer.com.au/

Numerical modeling of the development of kink-bands in anisotropic plastic materials

Dazhi Jiang

Laboratory for Structural Geology and Tectonics, Department of Geology, University of Maryland, College Park, MD 20742, USA

Email: dzjiang@geol.umd.edu

Tel: +1-301-405-6979, Fax: +1-301-314-7970

Paul F. Williams

Department of Geology, University of New Brunswick, P. O. Box 4400, Fredericton, NB E3B 5A3, Canada

Brooke L. Carter

Corresponding author

Keywords: kink band, anisotropic rheology, modeling, strain localization

Abstract: Kink-bands and associated kink folds are common structures in layered or foliated rocks. Their presence indicates that the dominant rheology of rocks was of anisotropic plasticity. We apply the commercial finite difference code FLAC and supplemental programs that we developed to address an outstanding problem of kink-band formation, namely what controls the onset and subsequent development of kink-bands. We use Mohr-Coulomb solid with an embedded planar anisotropy to simulate well-layered rocks. When subjected to anisotropy-parallel shortening, two competing deformation mechanisms are observed and their relative significance depends on the ratio (m) of the strength of the Mohr-Coulomb solid to that of the anisotropy. At a given strength of the solid, when m is low, the mode of deformation is strain localization leading to development of conjugate kink-bands. As m increases, strain localization gradually gives way to distributed deformation by kinking - formation of kink folds with axial planes at high angles to the shortening direction. Although as bulk strain increases, kink-band boundaries migrate through material and rotate to higher angles to the shortening direction, this migration and rotation is limited and is not the primary mechanism for kink fold development.

Table of Contents

Introduction and General Statement

Our knowledge of the rheology of the Earth's crust and lithosphere is a major limiting factor to our ability to model geodynamical processes and to interpret geological structures. While laboratory experiments on rock deformation provide invaluable constraints on rock rheology [e.g., Kohlstedt et al., 1995; Gleason and Tullis 1995], extrapolating experimentally determined results to time and spaces scales relevant for geodynamical models is nontrivial and introduces many uncertainties [e.g., Paterson 2001]. In addition, rheological anisotropy is ubiquitous in nature [e.g., Cobbold 1976; Lister and Williams, 1983], but is extremely difficult to be tackled experimentally. Approaches other than laboratory experiments that can yield rock rheological information are thus very useful. These include studies of 1) geological structures like faults and shear zones [e.g., Snoke and Tullis 1998] and fold geometries [e.g., Hudleston and Lan 1995], and 2) seismological and neotectonic studies of currently active fault systems [e.g., Rutter et al., 2001]. In this paper we follow the first approach. We investigate the mechanics for the development of a group of related structures - kink-bands and kink folds, which are common in upper crustal rocks and explore the use of their occurrence to constrain some aspects of the rock rheology.

Kink-bands [1] are common structures in well-layered and foliated rocks as well as anisotropic crystals. They are tabular zones or lenticular domains (kind-band domains, KBD's), generally with sharp boundaries (kink-band boundaries, KBB's), within which the penetrative planar feature (foliation in a rock or cleavage in a crystal) is rotated relative to its orientation outside of the zone (Figure 1). Within the KBD, the foliation may remain more or less planar (Figure 1a, b, c, and d , "simple kink-bands" in this paper) or may show further kinks (Figure 1e , "composite kink-bands" in this paper). Kink-bands may occur in a single set (Figure 1a, b, c, and e) or as a conjugate pair (Figure 1d). The geometry of the latter has rendered them being variably referred to as box folds, conjugate folds, or conjugate kinks [e.g., Paterson and Weiss, 1962; Hobbs, et al., p.210-211; Ramsay and Huber, 1987, p.319, 409, 420].

Figure 1. Kink-bands in rocks

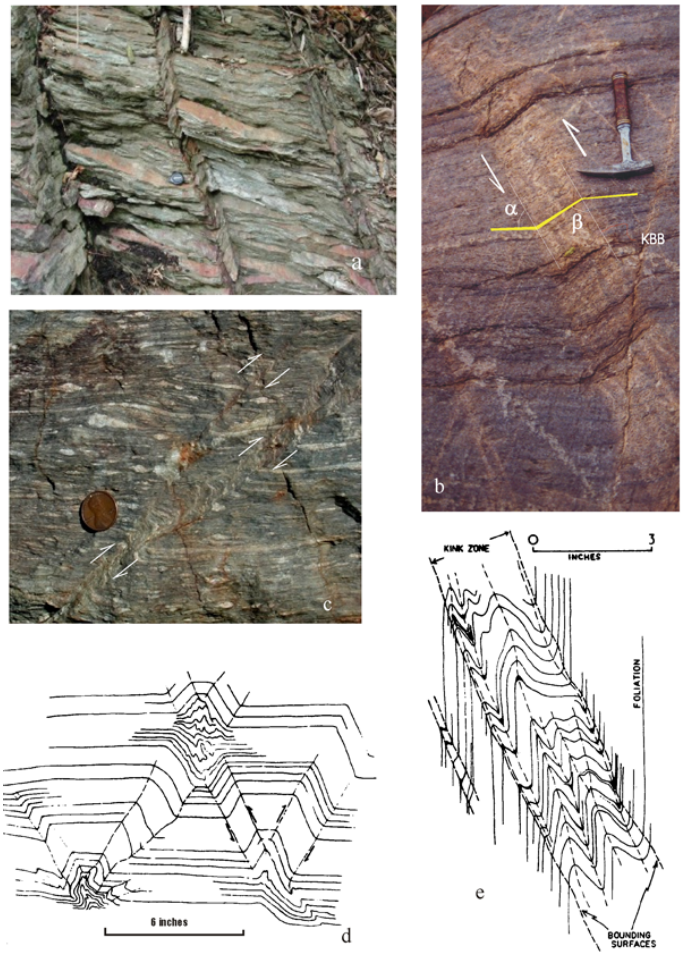

Kink-bands in rocks.

a. Kink-bands in metasiltstone at Harpers Ferry Maryland. Diameter of lens cap is 3cm.
b. Kink-bands in Huronian metasedimentary rocks, Espanola, Ontario.

[1]In this paper, we will use the term kink to describe any fold with straight limbs and angular hinge and use the term kink-band to describe a pair of kinks that include a short limb between two longer limbs. Typically the long limbs are at least an order of magnitude longer than the short limb. Formation of trains of kinks may involve similar foliation-parallel slip on alternating limbs, whereas foliation-parallel slip is probably restricted to, or is at least dominant in, the short limb in the formation of kink-bands. As we will demonstrate in this paper this genetic difference may be the fundamental difference between end member kink-bands (strain localization) and kinks (pervasive deformation). Geometrically there is a gradation from closely spaced kink-bands to asymmetrical kinks with limbs of similar length. Many natural examples of such kinks, from a genetic point of view, may be closely spaced kink-bands, which we have no way of telling. We therefore use the terms descriptively, restricting the term "kink-band" to the markedly asymmetric type, as described above, and to conjugate arrays of kink-bands which remain recognizable even when internal and external limbs approach similar length. All other morphologies are simply referred to as kinks.

c. Kink-bands in mylonite of the Garth Run shear zone in Madison County, Virginia. The mylonic C-foliation is cut by the kink-bands.
d. Conjugate kink-bands in Black Carboniferous slates on the southern side of the Beara Peninsula, Co. Cork, Ireland.
e. Composite kink-band at Creggan-a-tiadwar, central Murrisk, Co. Mayo, Eire. (d) and (e) are taken from Dewey (1965) with permission from Elsevier Science. See text for further discussion.

It is clear from laboratory experiments on slates and phyllites at room temperatures and various confining pressures [Paterson and Weiss 1962, 1966; Donath 1964, 1969; Anderson 1974] that, when subjected to foliation-parallel shortening, conjugate kink-bands will develop at relatively high confining pressures (e.g., > 300MPa, Anderson 1974), while fracturing occurs at lower confining pressures. The transition from kink-band development to fracturing may be also weakly strain-rate dependent according to experiments on salt-mica schist (W.D. Means per com). It is unclear how kink-bands originate and evolve. Paterson and Weiss (1962, 1966, 1968) proposed a kinematic model (Figure 2) whereby kink-bands start from a point or line source and grow in width by the KBB's migrating laterally into undeformed material. The process continues until conjugate kink-bands merge to form symmetric kinks and no undeformed regions are left in the material [see also Weiss 1980, Ramsay and Huber 1987, p.409]. Donath (1964, 1969) and Dewey (1965, 1969) maintain that KBB's are controlled by the principal stresses and are fixed to material particles after their initiation. The bounding KBB's of a kink-band separate until $b = 90°$ and then approach until $b = a$ (both angles are as defined in Figure 1b), when the kink-band "locks" and the mechanism is exhausted. Subsequent strain must be accommodated by development of new kink-bands or other mechanisms.

Figure 2. Kinematic model of Paterson and Weiss

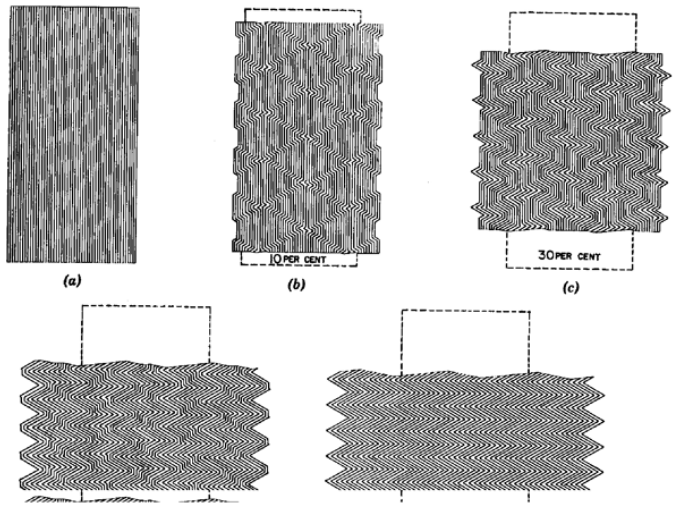

Kinematic model of Paterson and Weiss (1966) for kink-band development. Kink-band boundaries migrate until the whole rock is occupied by kinks. In this model kink-bands are earlier stage structures of kinks.

In the following we demonstrate with numerical finite difference modeling that the onset of kink-bands is a strain localization phenomenon necessarily controlled by rock rheology, stress state and deformation conditions, but the development of kink-bands after initiation is largely kinematic, with noticeable KBB migration and rotation. However, KBB migration does not consume the whole rock volume and is not a primary mechanism for the development of kink folds. Rather, kink-bands (strain localization) and kink folds (distributed strain) are produced by competing mechanisms governed by the degree of anisotropy of the rocks. Therefore we suggest 1) where kink-bands and/or kink folds are present the dominant rheological behavior at the time these structures were developed was likely plastic, and 2) the relative dominance of kink-bands and kink folds in a rock volume is an indicator of the degree of anisotropy of the rock.

Numerical Modeling with FLAC

General

FLAC (Fast Lagrangian Analysis of Continua, ICG, 1999) is a two-dimensional explicit finite difference program that is capable of solving a wide range of complex problems in continuum mechanics. It has been successfully applied to the study of a number of structural geology and rock mechanics problems such as strain localization

[Hobbs et al., 1990; Ord 1991; Poliakov and Herrmann 1994], quartz c-axis fabric development in folds [Zhang et al., 1993, 1994], single-layer buckling [Zhang et al., 1996, 2000], and asymmetric boudinage [Passchier and Druguet, 2002]. The new version 4.0 allows interactive grid generation, boundary condition and material property definition as well as graphic presentation of the results. In particular, FLAC contains a powerful built-in programming language FISH (short for FLACish) that allows the user to write his/her own programs to extend FLAC's functions including implementation of new constitutive models. FISH programs to derive kinematic histories of finite strain accumulation, vorticity, kinematic vorticity, and finite rotation have recently been developed in the Laboratory for Structural Geology and Tectonics at the University of Maryland. With these programs, it is possible to track the development history of any model-produced structures at required resolution.

Ubiquitous joint model to simulate foliated rocks in the plastic field

The following observations of natural kink-bands suggest that the most likely rheology for their development is one of anisotropic plasticity. First, kink-bands are most common in low-grade rocks such as slates and phyllites. They may occur in higher-grade rocks, but wherever they occur, they are commonly identified as being late in the deformation history [e.g., Dewey 1965]. In mylonites, for instance, they occur as a late structure overprinting the C-foliation (Figure 1b). All this suggests that kink-bands have developed in low temperature environments in which rocks likely behave like plastic solids. Second, the very fact that kink-bands occur mostly as localized *bands* suggests that they are strain localization phenomena. It is an intrinsic material property for most plastic materials to develop strain localization [e.g., Hobbs et al., 1990; Ord 1991; Vardoulakis and Sulem 1995]. For viscous materials to develop strain localization, some mechanisms of material softening such as those associated with mylonitization must be invoked [e.g., Poirier, 1980; White et al., 1980; Hobbs et al., 1990]. There is no microstructural evidence suggesting that these mechanisms have operated during kink-band development. Third, kink-bands are observed in well-foliated rocks or anisotropic crystals, suggesting that rheological anisotropy might be important in their formation.

Figure 3. Rheology of a Mohr-Coulomb

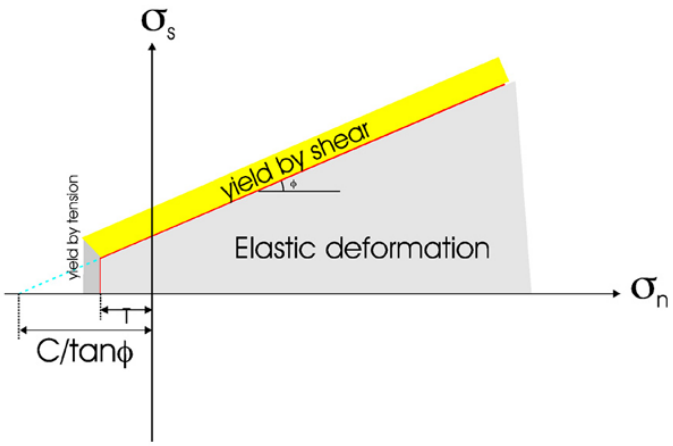

In FLAC modeling, the rheology of a Mohr-Coulomb solid is a Mohr-Coulomb criterion with a tension cutoff (ICG 1999, p.2-19). It deforms elastically (yellow area) unless the failure criterion is met when the solid fails either by shear or tension. See text for more discussion.

We use the Mohr-Coulomb model to simulate plasticity, and the ubiquitous joint model to simulate anisotropy. A Mohr-Coulomb solid behaves elastically unless the Mohr-Coulomb yield criterion is satisfied (Figure 3). The material yields either by shear, for which the envelope criterion is:

$$\sigma_s = C + \tan\phi\,\sigma_n$$

or by tension, for which the criterion is:

$$\sigma_3 = -T$$

In equations 1 and 2, s_s and s_n are shear and normal stresses respectively, and s_3 is the minimum principal stress (compressive stress is taken positive); C, f, and T are, respectively, the cohesion, friction angle, and the tensile strength of the material.

$$\tau \le \frac{C}{\tan \phi} \qquad \tau_j \le \frac{C_j}{\tan \phi_j}$$

The ubiquitous joint model in FLAC is a Mohr-Coulomb plastic solid with an embedded penetrative weak plane (ubiquitous joint) of specific orientation. When a well-layered or foliated rock is viewed on the scale in which the layering or foliation is truly penetrative, the rheology of the rock can be simulated by the ubiquitous joint model. One can regard the rheology of the microlithon domain as the Mohr-Coulomb solid, and the foliation septum the ubiquitous joint. In a ubiquitous joint model, plastic yielding may occur either in the Mohr-Coulomb solid or along the weak plane, or both, depending on the stress state, the orientation of the weak plane and the material properties of the solid and the weak plane. The yield criteria of the weak plane (ubiquitous joint) are:

$$\sigma_s = C_j + \tan \phi_j \sigma_n$$

$$\sigma_3 = -T_j$$

where the subscript j stands for ubiquitous joint, and:

It can be readily seen that the ubiquitous joint model represents the simplest anisotropic plastic material, one with an axial symmetry. For such a material, similar to Ramsay and Lisle (2000, p. 778) and Treagus (2002), a parameter, m, can be defined to measure the degree of anisotropy. m is defined as the ratio of the shear strength of the Mohr-Coulomb solid to that of the weak plane:

$$m = \frac{C + \tan \phi \sigma_n}{C_j + \tan \phi_j \sigma_n}$$

Clearly, $m=1$ represents the situation that the ubiquitous joint has the same strength as, and is mechanically indistinguishable from, the solid. The material is therefore isotropic. As m increases, the material becomes more anisotropic.

For rocks, the range of variation of C_j and C is from 10MPa to tens of MPa [e.g., Carmichael 1989]. The confining pressures under which kind-bands develop are well above 100MPa (>300MPa according to Anderson 1974). Therefore for conditions relevant to kink-band development, the stress conditions are always $s_n >> C$ or C_j . This can be used to simplify equation 5 to:

$$m \approx \frac{\tan \phi}{\tan \phi_j}$$

In the following, we present our modeling investigation on how the deformation mode of a ubiquitous joint model varies as m varies for given sets of material properties.

Model Setup and Modeling Procedure

In FLAC modeling, the solid body ("sample") is divided into a finite difference mesh composed of quadrilateral elements, called zones. In FLAC's actual calculation, a zone is subdivided into 2 sets of triangles (Figure 4). A quadrilateral zone may be deformed in any fashion, subject to (1) the area of the quadrilateral being positive, and (2) each member of at least one pair of triangles being >20% of the total quadrilateral area. If either criterion is violated, FLAC issues an error message of "bad geometry" and the modeling cannot proceed further. This limits the amount of bulk strain that can be reached for some numerical runs.

The geometry of the model setup is schematically shown in Figure 5 . A homogeneous Mohr-Coulomb body of 100m by 100m containing a horizontal ubiquitous joint (anisotropy plane) is subjected to shortening parallel to the anisotropy. A displacement boundary condition is applied and the specimen is confined under a pressure of 500MPa throughout deformation. The lateral boundaries are frictionless (Figure 5). A grid size of 1 meter by 1 meter is used (that is the sample has in total 10,000 equal sized zones). We have tested possible effects of grid size on modeling results by reducing the zone size to 0.5m by 0.5m for some numerical runs, and the results are quantitatively identical to those with a grid size of 1m by 1m. All results presented below are for 1m by 1m grid size situations.

Figure 4. FLAC numerical modeling

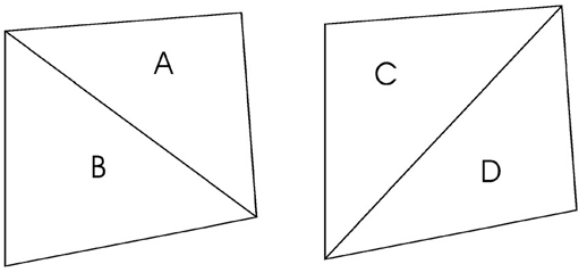

In FLAC numerical modeling the sample is divided into a finite difference mesh of quadrilateral elements called zones in which the deformation is homogeneous. Each zone is subdivided into 2 pairs of triangles (A and B, C and D). The distortion of a zone must be within certain limits so that the zone does not run into "bad geometry". See text for more discussion.

Figure 5. Geometric setup of the numerical modeling

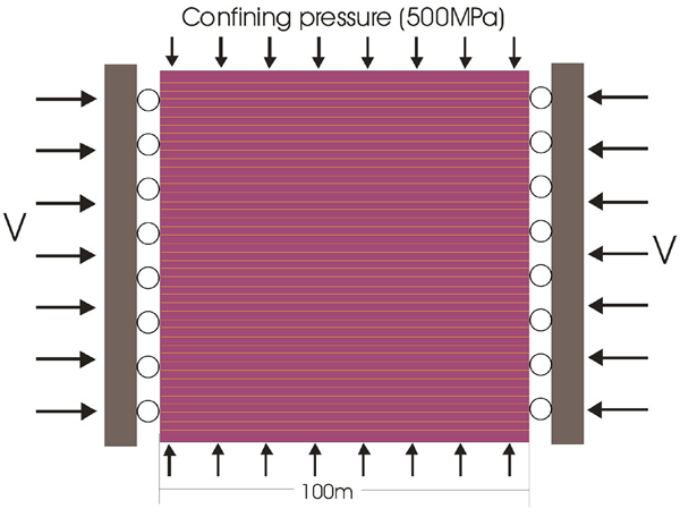

Geometric setup of the numerical modeling. See text for details.

The following material properties for the Mohr-Coulomb solid compiled from the rock type shale of Carmichael (1989) are used: density 2500kg/m^3, bulk modulus 2.81x10^4 MPa, shear modulus 1.69x10^4 MPa, cohesion (C) 3.0MPa, tensile strength (T) 1.5 MPa, friction angle (ϕ) 30°, and dilation angle (for definition see Ord 1991) 4°. Mechanical properties of the ubiquitous joint ("foliation") are: cohesion (C_j) 7.5x10^{-3} MPa, tensile strength (T_j) 4x10^{-3} MPa. The friction angle (ϕ_j) for a specific modeling run is calculated according to equation 6 for a given

m value. An incremental displacement of 1mm per step is used, which means that for every 1000 steps, 1% of bulk shortening is achieved. A specimen is shortened to as high a strain as possible, until a zone develops "bad geometry".

At the end of a model run, the grid coordinates of points whose history is of interest are identified. The model is then rerun with the histories of marked points recorded using FISH programs developed at Maryland.

Results for Fixed Bulk Strength and Varied Degree of Anisotropy

Progressive geometrical evolution

Figs. Figure 6 , Figure 7 , Figure 8 , and Figure 9 show progressive evolution of the specimen as deformation advances for four numerical experiments identical in all respects except the m values. The banding in these figures serves as passive markers parallel to the anisotropy. They do not have any mechanical significance. The following observations are readily made from these figures.

When m = 2 (Figure 6), the modeling reaches a maximum bulk shortening of 11%. Conjugate kink-bands develop. They are simple kink-bands. α α 40° when the kink-bands are clearly defined at 8% shortening. Kink bands rotate slightly as strain increases (α α 42° at 11% of strain). KBB's migration is clearly indicated by widening of kink-bands as deformation advances (Figure 6a and b) and by the concentration of incremental strain at KBB's. As kink-bands widen, b increases from 0 to being close to a. Foliation within the KBD remains planar. Outside the kink-bands, the foliation remains planar and the strain is low (~4%, Figure 10 , see below). Figure 6c is a contour map of the instantaneous shear-strain increment per step, the second invariant of the incremental strain tensor, at the instant the bulk strain is 10%. It shows that as b approaches a, active deformation occurs only at the migrating kink-band boundaries; the interior of the band is practically inactive. Both bounding boundaries of a kink-band may be migrating (solid white arrows in Figure 6c), or only one boundary is (open white arrows in Figure 6c).

Figure 6. Modeling results for m=2

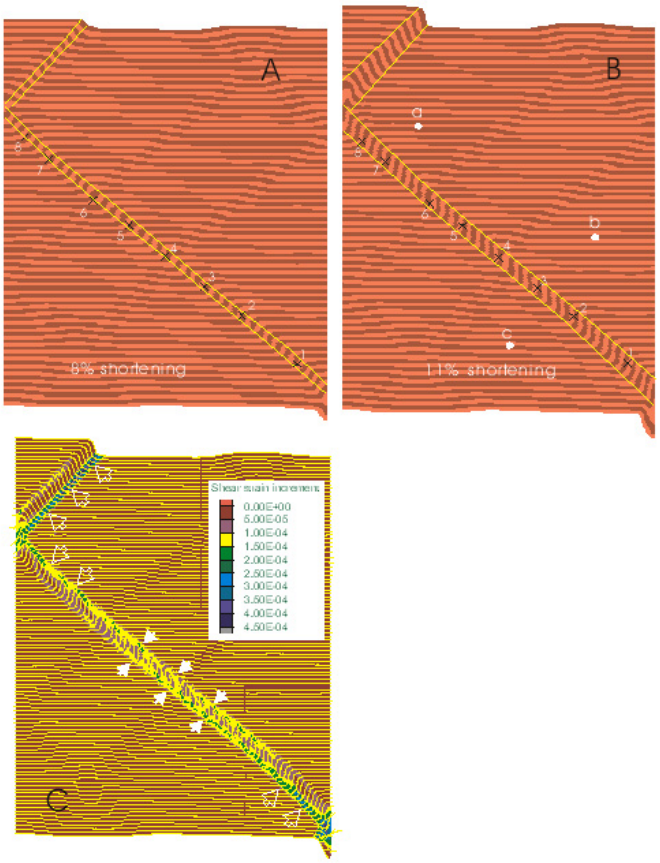

Modeling results for m = 2. (A) Conjugate kink-bands occur as strain localization bands. (B) Kink-bands widen by migration of kink-band boundaries. (C) The incremental shear strain of at the state when bulk shortening is 10%. High-shear incremental shear strains are at both kink-band boundaries (solid white arrows), or one kink-band boundary only (open white arrows). Yellow lines are the orientation of ubiquitous joints. Numbered and lettered gridpoints are those whose stress and strain histories are recorded (Fig. 10).

Figure 7. Modeling results for m=5

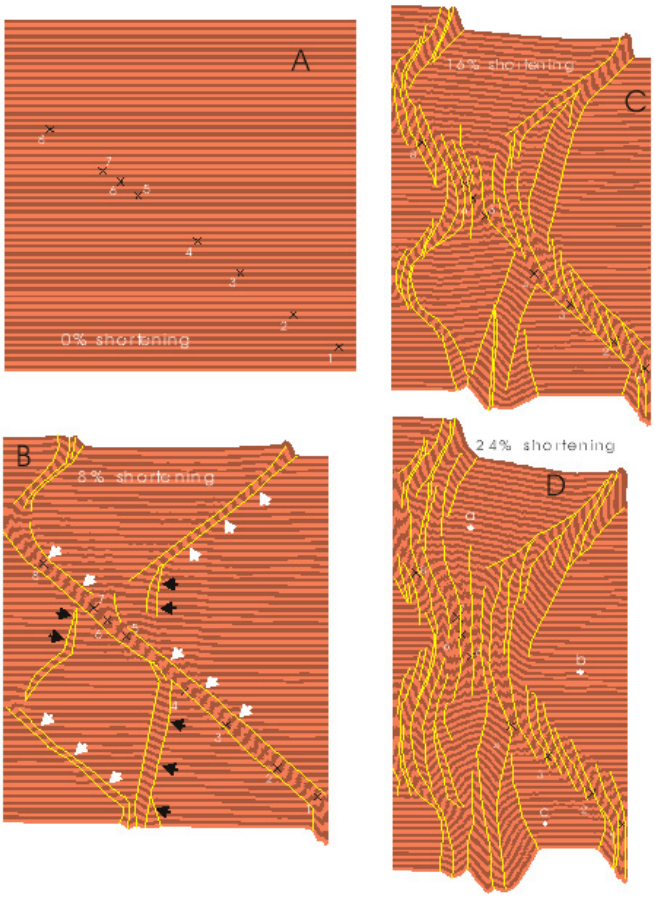

Modeling results for m=5. (A) The undeformed state. (B) At 8% of shortening, both conjugate kink-bands (white arrows) and high-angle kink-bands are initiated as strain localization zones. The former are composite kink-bands. (C) Migration of kink-bands is clear. Within conjugate kink-bands, kinks have their axial planes in an en echelon array. High-angle bands develop into kinks. (D) Kink-bands continue to widen and kinks tighten as bulk shortening advances.

When m=5 (Figure 07), at a low value of bulk shortening (8%), conjugate kink-bands (white arrows in Figure 7b), as well as kink-bands at higher angle to the foliation (high-angle bands hereafter, black arrows in Figure 7b) develop. Unlike m=2 case, the conjugate kink-bands are composite bands (with further kinks in them). As bulk shortening further increases (16% and 24%), all kink-bands widen, and more new high-angle bands emerge. Earlier high-angle bands evolve into kink folds or box-like folds (bottom part in Figure 7c and d). Thus the high-angle bands are initial stages of kink and box-type folds. Kinks within conjugate kink-bands have their axial planes arranged en echelon within their hosting bands, consistent with the sense of shear of the hosting kink-bands. As shortening increases, all bands rotate toward higher angles with respect to the shortening direction. Merging of conjugate kink-bands is observed only in the vicinity of the intersection of two conjugate bands.

As m is further increased (m=10, Figure 08), strain-localization-type conjugate kink-bands observed in Figures 6 and 7 are absent. Only high-angle bands kinks with axial planes close to normal to the shortening direction, develop. At low strains (e.g., <16% shortening, Figure 8a and b), one can identify a broad zone of concentrated kinks in the orientation of conjugate kink-bands Figure 8a . When m=20 (Figure 9), the deformation is achieved completely by pervasive kinking throughout the specimen.

Figure 8. Modeling results for m=10

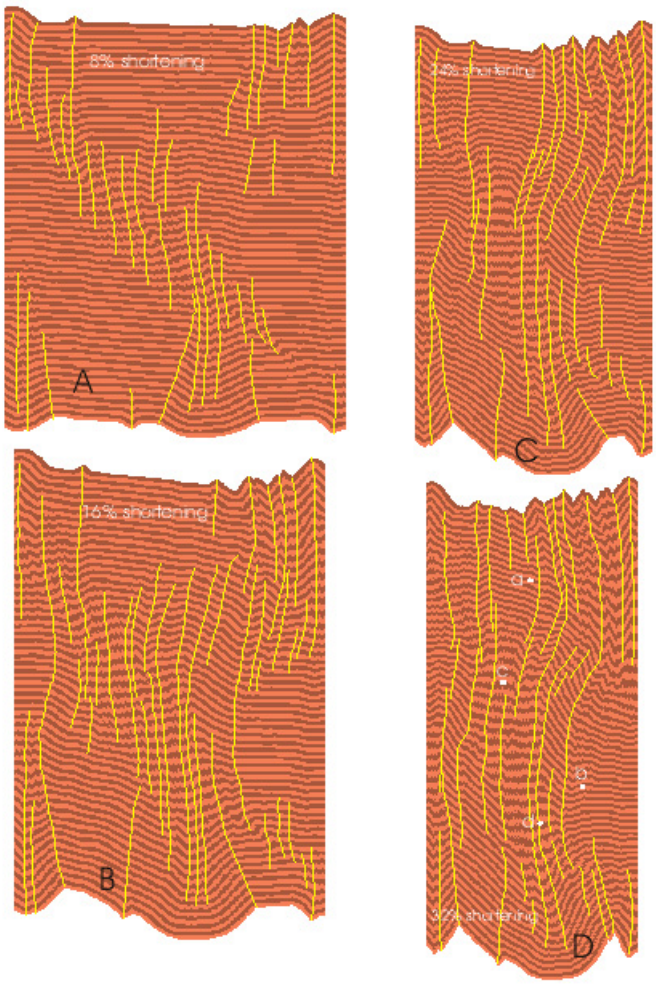

Strain-localization type bands do not develop. Only kinking occurs, but kinks concentrate in a broad zone in the orientation of conjugate kink-bands at low strains (A). As strain increases (B, C, and D) this zone is obscured and overall geometry resembles symmetric kinks.

Figure 9. Modeling results for m=20

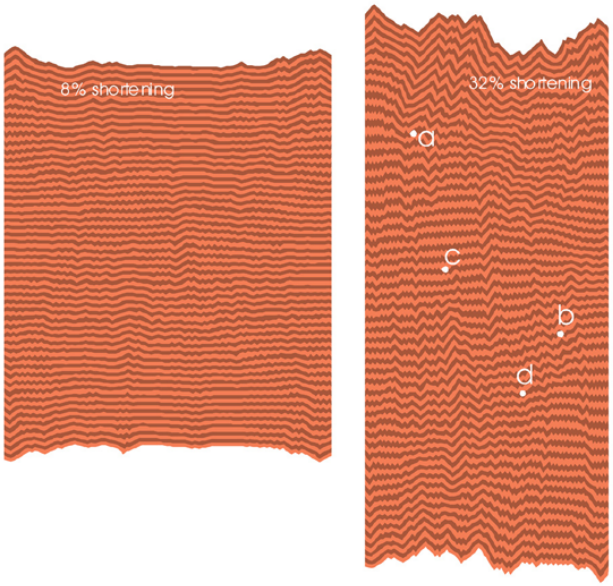

The mode of deformation is entirely kinking in the whole volume of the specimen.

Stress and strain histories

In order to determine the history of kink-band development and examine whether kink-bands develop from a point source, we select a number of material points inside and outside of a kink-band from the final configuration of modeling runs (numbered and lettered grid points in Figures 6, 7, 8, and 9), identify their grid coordinates, and rerun the modeling to record the stress and finite strain histories of these points. A FISH program 'strain_his" was developed to retrieve the history of $R_f = (1 + e_1) / (1 + e_3)$ where e_1 and e_3 are respectively the two principal elongations) for selected points.

Figures 10 and 11 are plots of the accumulation of finite strains for m=2 and m=5 cases respectively. Points 1 through 8 are inside a kink-band and points a, b, and c outside of the kink-band (Figures 6 , 7). Outside the kink-band domain, finite strain increases to a low value and remains nearly constant thereafter (Figure 10b and Figure 11b). The maximum strain ratio outside kink-bands is around 1.1, except for point a in the m=5 case (Figure 11b), for which the higher strain is interpreted as being due to development of local kinking. $R_f = 1.1$ corresponds to principal elongation values of e_1=4.4% and e_3=-4.2%, which are close to the bulk shortening value at the time the kink-band starts to develop (Figure 10a and Figure 11a). This implies that for m=2 and m=5 cases, once kink-bands start to develop, strain remains approximately constant outside kink-bands. That is, deformation is nearly entirely localized into kink-bands.

Figure 10. History of finite strain accumulation (m=2)

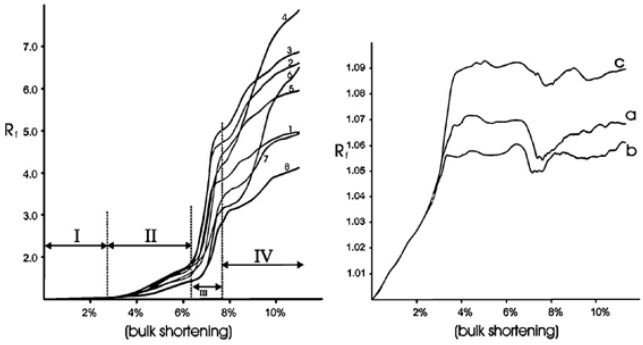

History of finite strain accumulation for gridpoints inside (1 through 8) and outside (a, b, and c) a kink-band for m=2 case. Strain outside the kink-band remains approximately the same after kink-bands are initiated. Strain inside kink-bands increases rapidly after kink-bands are initiated. See text for further discussion.

Figure 11. History of finite strain accumulation (m=5)

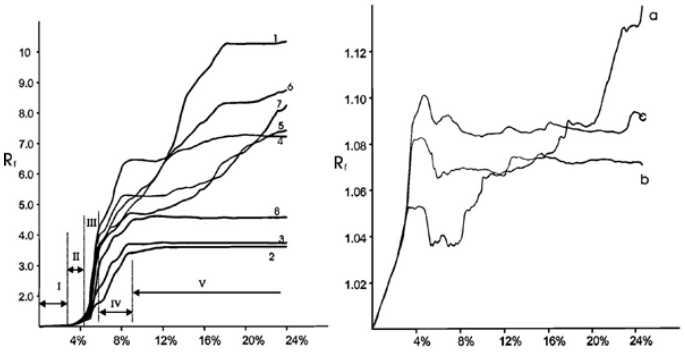

History of finite strain accumulation for gridpoints inside (1 through 8) and outside (a, b, and c) a kink-band for m=5 case. Following initiation of kink-bands, strain outside the kink-band remains approximately the same but increases rapidly inside the band until the kink-band "locks" (stage V). See text for further discussion.

We describe the accumulation of finite strain inside the KBD in terms of 5 stages (Figs. 10A and 11A). Stage I evidently corresponds to homogeneous elastic deformation throughout the sample. In stage II finite strain increases at

an increased rate, corresponding to the initiation of kink-bands. This stage is followed by stage III, an accelerated increase in the rate of finite strain accumulation, marking the instability associated with kink-band formation. All marked grid points inside the kink-band follow similar strain increase path, suggesting that strain localization rather than kinematic growth from a line or point source is responsible for the onset of kink-bands. Following stage III, the rate of strain increase is reduced and, if the sample can be deformed further without running into "bad geometry" (m=5 case), strains at many points may reach a maximum value and then cease to increase (stage V, Figure 11a). We interpret this as indicating the "lock-up" of kink-bands.

In terms of stress history (Figure 12), for both m=2 and m=5 cases, the initiation of kink-bands is marked by a drop in axial stress followed by a further accelerated drop in axial stress. The initial stress drop is interpreted as being due to yielding of the Mohr-Coulomb solid and the accelerated drop is interpreted as being due to yielding along the anisotropy and localization of strain into kink-bands. Following that, the axial stress climbs up to a level close to the initial yielding (peak) stress for the m=2 case. Further evolution of the stress is unclear for them=2 case because the modeling was terminated at 11% bulk shortening due to "bad geometry". We speculate that the stress most likely will exhibit cyclic fluctuations as schematically shown in m=2 case of Figure 13 , as new kink-bands develop continually. For the m=5 case (Figure 12), after the stress drop associated with kink-band instability, the axial stress climbs up to a level noticeably below the initial yielding stress and then fluctuates at this level. We interpret this as being associated with kinking outside kink-bands as well as broadening of KBD's (Figure 6 , Figure 13 m=5 case).

Figure 12. History of axial (horizontal normal) stress

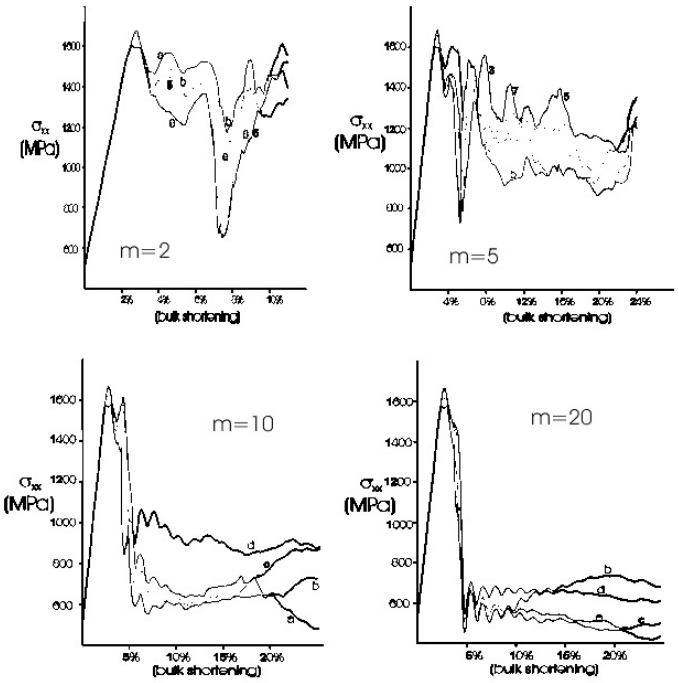

History of axial (horizontal normal) stress for marked gridpoints for the four numerical experiments of m=2, 5, 10, and 20. See text for discussion.

Figure 13. Simplified and schematic stress-strain

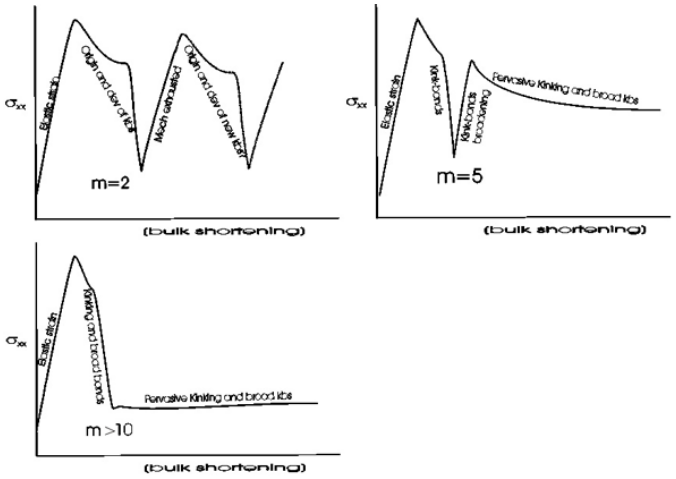

Simplified and schematic stress-strain curves for low (m=2), intermediate (m=5), and high (m>10) degree of anisotropy. See text for discussion.

As the material becomes more anisotropic (the m=10 and 20 cases), the stress history is different in two respects (Figure 12 , m=10 and 20 cases). First, the separation between the initial drop in axial stress, interpreted as marking

the yield of the Mohr-Coulomb solid, and the drop interpreted as yielding of the foliation, is strongly subdued (for the m=10 case) or barely visible (for the m=20 case). This suggests a rapid transition from yielding of the solid to yielding of the foliation. Second, the climb-up of stress following yielding is almost absent. The axial stress fluctuates at a very low level (close to the confining pressure for the m=20 case), corresponding to pervasive kinking. This indicates that, if a material is highly anisotropic, it cannot support high differential stress once the foliation is kinked (Figure 13 , m> 10 case).

Factors Controlling Kink-band Development: Deformation mechanism map

A ubiquitous joint body used to simulate well-foliated rocks needs 11 material parameters for complete characterization, of which 7 are for the Mohr-Coulomb (bulk) solid (density, bulk modulus, shear modulus, cohesion, tensile strength, friction angle, and dilation angle) and 4 are for the ubiquitous joint (anisotropy) (cohesion, tensile strength, friction angle and dilation angle). They all affect the deformation of the material. However, density and elastic constants (bulk and shear modules) for rocks are well determined from laboratory experiments and they do not vary significantly for conditions under which kink-bands develop. The range of variation of cohesion in rocks is also limited. The parameters that affect deformation the most are the friction angle of the Mohr-Coulomb solid and the friction angle of the ubiquitous joint. Therefore, to a first order approximation, for kink-band situations, the ubiquitous joint model can be characterized by two parameters: the bulk strength measured by the internal friction angle of the Mohr-Coulomb solid, and the degree of anisotropy. We have carried a lot more numerical experiments with varied friction angles of the Mohr-Coulomb solid and m-values. A transition in deformation mode from strain localization (development of kink-bands), to distributed deformation (kinking), as shown in Figures 6-9, is always observed as f is kept constant and m is increased. We present three more numerical experiments (for m=2, 8, and 10, respectively) for material properties identical to those for Figures 6-9 except that the internal friction is reduced to f = 20° here as animations (Animation 1 , Animation 2 , and Animation 3), and the transition from one dominant mode of deformation to another as a deformation mechanism map (Figure 14). Since the transition from one dominant mechanism to another is gradual, the boundaries between the mechanism domains are transitional.

Figure 14. Deformation mechanism map

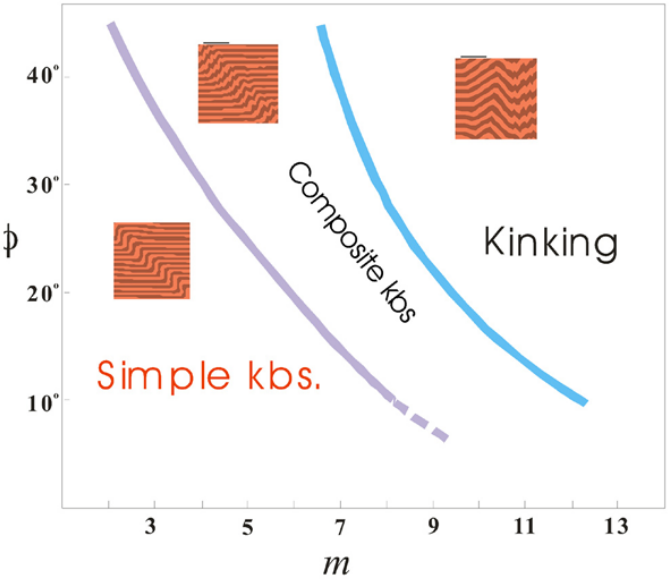

Deformation mechanism map showing the transition of mode of deformation from simple kink-bands through composite kink-bands to symmetric kinks as function of the degree of anisotropy and bulk strength of the Mohr-Coulomb solid. See text for more detail.

Figure 1. Numerical experiment for m = 2

Numerical experiment (for m = 2) for material properties identical to those for Figures 6-9 except with the internal friction reduced to f = 20°.

Figure 2. Numerical experiment for m = 8

Numerical experiment (for m = 8) for material properties identical to those for Figures 6-9 except with the internal friction reduced to f = 20°.

Figure 3. Numerical experiment for m = 10

Numerical experiment (for m = 10) for material properties identical to those for Figures 6-9 except with the internal friction reduced to f = 20°.

Discussion and Implications

Modeling results summarized above confirm that kink-bands are strain localization bands and as such their initiation is necessarily controlled by the rheology of the material, stress state and deformation conditions. Once initiated, subsequent evolution of kink-bands is largely

kinematic. Kink-band boundaries migrate through the material, rotate to unfavorable orientations and cease to operate as a deformation mechanism as strain increases. New kink bands are continually developed. To develop kink-bands, the material must not be too anisotropic for high degree of anisotropy will favor pervasive kinking at the expense of localized kink-bands. Kink-bands and kinks are products of competing mechanisms (Figure 14). The latter do not result from widening of the former.

The deformation mechanisms map can be readily applied to natural kink-bands. Friction angles of common rock types are experimentally constrained [e.g., Carmichael 1989]. By examining the geometry of kink-bands and kinks in an area, one can use Figure 14 to estimate of the degree of anisotropy of the rock.

An anisotropic rock is often more complicated than a ubiquitous joint body. First the ubiquitous joint model has an axial symmetry because in the plane of the ubiquitous joint there is no rheological difference. A rock may, however, have a linear fabric in addition to a foliation and therefore exhibit anisotropy lower than axial. Second, the rheology of a rock may change during the course of deformation. For example, a rock behaving viscously under high-grade metamorphic conditions may be transiently plastic if the fluid pressure is elevated due to partial melting or dehydration metamorphic reaction, leading to significant reduction of the effective confining pressure. If the rock has a planar fabric as well, kink-bands and kink folds may accordingly develop even though the dominant rheology of the rock is in the viscous field.

Conclusions

There are two competing mechanisms of deformation in plastic anisotropic materials: One is strain localization, leading to development of kink-bands, and the other is distributed deformation of kinking. As the degree of anisotropy and the bulk strength vary, there is a gradual transition from localization forming simple kink-bands, to localization forming composite kink-bands, to diffused deformation forming symmetric kinks. The relative significance of localized kink-bands and diffused kinks allows one to estimate the degree of anisotropy of the rock at the time the structures were formed.

As a strain-localization phenomenon, the onset of kink-bands is controlled by rheology, stress state and deformation conditions, but subsequent development of kink-bands is largely kinematic. Kink-band boundaries migrate through material and rotate toward higher angles to the shortening direction as deformation advances. However, kink-band boundary migration is limited and does not lead to formation of kinks except in areas where a pair of conjugate kink-bands intersect.

Kinks are produced by folding of the anisotropy with axial planes close to 90 with respect to the shortening direction. Like kink-band boundaries, such axial planes may migrate through material as deformation advances.

Acknowledgments

DJ and PFW thank Dr. Yanhua Zhang for tutorial of FLAC during their visit to CSIRO in the summer of 2000. We thank Bruce Hobbs, Alison Ord, Hans Muhlhaus, and Michael Brown for helpful discussion. This work was supported by NSF (EAR0003315) and American Chemical Society Petroleum Research Fund to DJ.

References

Anderson, T. B. 1974. The relationship between kink bands and shear fractures in the experimental deformation of slate. Journal of Geological Society of London 130, 367-382.

Carmichael, R. S. 1989. Practical Handbook of Physical Properties of Rocks and Minerals. CRC Press, Boston.

Cobbold, P.R. 1976. Mechanical effects of anisotropy during large finite deformations. Bulletin of the Society of Geologists, France 18, 1497-1510.

Dewey, J. 1965. Nature and origin of kink-bands. Tectonophysics 1, 459-494.

Dewey, J. 1969. The origin and development of kink bands in a foliated body. Geological Journal 6, 193-216.

Donath, F. A. 1964. Strength variation and deformational behaviour in anisotropic rocks. In: W. R. Judd (ed) State of stress in the Earth's crust. Elsevier, NY 281-300.

Donath, F. A. 1969. Experimental study of kink-band development in Martinsburg slate. Geological Survey of Canada Paper 65-52, 255-292.

Gleason, G.C. and Tullis, J. 1995. A flow law for dislocation creep of quartz aggregates determined with the molten salt cell. Tectonophysics 247, 1-23.

Hobbs, B. E., Means, W. D. and Williams, P. F. 1976. An outline of structural geology. John Wiley, New York.

Hudleston, P.J. and Lan, L. 1995. Rheological information from geological structures. Pure and Applied Geophysics 145, 605-620.

Hobbs, B. E., Mühlhaus, H. -B., and Ord, A. 1990. Instability, softening and localization of deformation. In: Knipe, R. J. & Rutter, E. H. (eds.) "Deformation Mechanisms: Rheology and Tectonics", Geological Society, London, Special Publication 54, 143-165.

ICG (Itasca Consulting Group, Inc.), 1999. FLAC: Theory and Background. Minneapolis, Minnesota.

Jiang, D. and White, J. C. 1995. Kinematics of rock flow and the interpretation of geological structures, with particular reference to shear zones. Journal of Structural Geology 17, 1149-1165.

Kohlstedt, D. L., Evans, B. and Mackwell, S.J. 1995. Strength of the lithosphere: constraints imposed by laboratory experiments. Journal of Geophysical Research 100, 17, 587-17,602.

Ord, A. 1991. Deformation of rock: a pressure-sensitive, dilatant material. Pure and Applied Geophysics 137, 337-366.

Passchier, C. W. and Druguet, E. 2002. Numerical modeling of asymmetric boudinage. Journal of Structural Geology 24, 1789-1803.

Paterson, M. 2001. Relating experimental and geological rheology. International Journal of Earth Sciences 90, 157-167.

Paterson, M. S. and Weiss, L. E. 1962. Experimental folding in rocks. Nature 195, 1046-1048.

Paterson, M. S. and Weiss, L. E. 1966. Experimental deformation and folding in phyllite. Geological Society of America Bulletin 77, 343-374.

Paterson, M. S. and Weiss, L. E. 1968. Folding and boudinage of quartz-rich layers in experimentally deformed phyllite. Geological Society of America Bulletin 79, 795-812.

Poliakov, A.N.B. and Herrmann, H. J. 1994. Self-organized criticality of plastic shear bands in rocks. Geophysical Research Letters 21, 2143-2146.

Poirier, J. P. 1980. Shear localization and shear instability in materials in the ductile field. Journal of Structural Geology 2, 135-142.

Ramsay, J. G. 1967. Folding and fracturing of rocks. McGraw-Hill, New York.

Ramsay, J. G. 1974. Development of chevron folds. Geological Society of America Bulletin 85, 1741-1754.

Ramsay, J. G. and Huber, M. I. 1987. The Techniques of Modern Structural Geology, Vol. 2. Folds and Fractures. Academic Press, London.

Ramsay, J.G. and Lisle, R.J. 2000. The Techniques of Modern Structural Geology, Vol. 3. Applications of Continuum Mechanics in Structural Geology. Academic Press, London.

Rutter, E. H., Holdsworth, R.E. and Knipe, R.J. 2001. The nature and tectonic significance of fault-zone weakening: an introduction. In: Holdsworth, R.E., Strachan, R.A., Magloughlin, J.F. and Knipe, J. F. (eds) “The Nature and Tectonic Significance of Fault Zone Weakening” Geological Society, London, Special Publication 186, 1-11.

Snoke, A. and Tullis, J. 1998. An overview of fault rocks. In: Snoke, A., Tullis, J. and Todd, V. R.(eds.) “Fault-related Rocks: A Photographic Atlas”, Princeton University Press, New Jersey.

Treagus, S.H. 2002. Modelling the bulk viscosity of two-phase mixtures in terms of clast shape. Journal of Structural Geology 24, 57-76.

Vardoulakis, I., and Sulem, J. 1995. Bifurcation Analysis in Geomechanics. Chapman and Hill.

Weiss, L. E. 1980. Nucleation and growth of kink bands. Tectonophysics 65, 1-38.

White, S. H., Burrows, S. E., Carreras, J., Shaw, N. D., and Humphreys, F. J. 1980. On mylonites in ductile shear zones. Journal of Structural Geology 2, 175-187.

Zhang, Y., Hobbs, B. E. and Jessell, M. W. 1993. Crystallographic preferred orientation development in a buckled single layer: a computer simulation. Journal of Structural Geology 15, 265-276.

Zhang, Y., Hobbs, B. E. and Jessell, M. W. 1994. The effect of grain boundary sliding on fabric development in polycrystalline aggregates. Journal of Structural Geology 16, 1315-1325.

Zhang, Y., Mancktelow, N. S., Hobbs, B. E., Ord, A. and Mühlhaus, H. B. 2000. Numerical modeling of single-layer folding: clarification of an issue regarding the possible effect of computer codes and the influence of initial irregularities. Journal of Structural Geology 22, 1511-1522.

Zhang, Y., Hobbs, B. E., Ord, A. and Muhlhaus, H. B. 1996. Computer simulation of single-layer buckling. Journal of Structural Geology 18, 643-655.